Inner-shell photoionization of group-IIB atoms

M. Kutzner, C. Tidwell, and S. E. Vance
Physics Department, Andrews University, Berrien Springs, Michigan 49104

V. Radojević
Institute of Physics, P.O. Box 57, 11000 Belgrade, Yugoslavia

Total and partial photoionization cross sections, branching ratios, and angular-distribution asymmetry parameters for inner subshells $(nl, l \geq 2)$ of the group-IIB elements zinc, cadmium, and mercury have been calculated in both the relativistic random-phase approximation and the relativistic random-phase approximation modified to include relaxation. Comparisons are made between the results of the two theoretical methods and with experiment where available. The present theoretical results for the $3d$ inner-shell photoionization of zinc are not in accord with experiment. We confirm previous work [S. L. Carter and H. P. Kelly, J. Phys. B **11**, 2467 (1978)] which demonstrated that relaxation is an important effect in photoionization of the $4d$ subshell of atomic cadmium. It is also found that the inclusion of relaxation effects resolves a discrepancy between theory and experiment for the $4f$ inner-shell photoionization of atomic mercury.

PACS number(s): 32.80.Hd, 32.80.Fb

I. INTRODUCTION

The study of inner-shell photoionization of many elements has led to an improved understanding of a number of interesting many-body phenomena including relaxation and polarization effects, the Auger effect, photoionization with excitation, and multiple photoionization. The importance of relaxation has long been established in the photoionization of $3d$ and $4d$ subshells of elements from xenon $(Z = 54)$ through the lanthanides. In previous papers [1,2], the relativistic random-phase approximation (RRPA), which includes many of the effects of electron correlation, and the relativistic random-phase approximation modified to include relaxation effects (RRPAR) were applied to calculations of inner-shell photoionization of the alkaline-earth metal atoms group-II A. The results of those studies showed that relaxation effects were not large for the alkaline-earth metal atoms Be through Sr, but that the effects were large for both the $4d$ and $3d$ subshells of atomic Ba. It was also noted that including relaxation in the calculation often altered the partial subshell cross section more than the total photoionization cross section. The group-IIB elements differ from the group-II A elements in that the valence subshell ns^2 is preceded by the filled d subshell $(n-1)d^{10}$ rather than a filled p subshell $(n-1)p^6$. Based on the results of the alkaline-earth calculations [1,2], it is anticipated that the shape resonances resulting from photoionization of the penultimate subshells of the group-IIB elements, $(n-1)d^{10}$, should be modified by the effects of core relaxation.

The least studied of the group-IIB elements is atomic zinc $(Z = 30)$ with ground state $[Ar]3d^{10}4s^2$. The total photoionization cross section of Zn above the $3d$ thresholds was measured by Harrison, Schoen, and Cairns [3] in 1969 and partial cross sections have been

reported by Süzer et al. [4]. Walker et al. [5] and Süzer et al. [4] have measured the branching ratio $\gamma = \sigma(3d_{5/2})/\sigma(3d_{3/2})$ for a few points. The measured total cross section [3] disagreed with an RRPA calculation of Johnson, Radojević, and Deshmukh [6], a discrepancy which has yet to be resolved.

More work has been done on cadmium $(Z = 48)$ with a ground state $[Kr]4d^{10}5s^2$. The total cross section above the $4d$ thresholds has been measured by Cairns, Harrison, and Schoen [7] and Codling, Hamley, and West [8]. Very recently, von Garnier et al. [9] have measured the partial $4d$ cross section of Cd as well as satellite intensities in this region. Experimental branching ratios $\gamma = \sigma(4d_{5/2})/\sigma(4d_{3/2})$ have been reported by von Garnier et al. [9], Shannon and Codling [10], Süzer, Lee, and Shirley [11], Walker et al. [5], and Kobrin et al. [12]. Experimental asymmetry parameters β_{4d} have been reported by von Garnier et al. [9], Schönhense [13], Kobrin et al. [12], and Theodosiou et al. [14]. Theoretical calculations of the partial $4d$ photoionization cross section using the many-body perturbation theory (MBPT) have been carried out by Carter and Kelly [15], who found significant effects due to the correct treatment of exchange and core relaxation. Dirac-Fock calculations of Tambe, Ong, and Manson [16] confirmed the findings of MBPT. RRPA calculations [6] yield results similar to the calculations of Carter and Kelly [15] that did not include relaxation.

Atomic mercury $(Z = 80)$ with a ground state $[Xe]4f^{14}5d^{10}6s^2$ is the heaviest stable element with closed electronic subshells and an appreciable vapor pressure at low temperatures [17]. It has been the subject of numerous inner-shell photoionization studies. Total photoionization cross sections above the Hg $5d$ threshold have been measured by Cairns, Harrison, and Schoen [18] and Süzer et al. [4]. The total cross section has been partitioned into partial cross sections near the $5d$ threshold

by Shannon and Codling [10] and Dehmer and Berkowitz [19] and at higher energies by Lindle *et al.* [20]. Branching ratios $\gamma = \sigma(5d_{5/2})/\sigma(5d_{3/2})$ have been experimentally determined by numerous workers [4,10,11,17,19,21] and asymmetry parameters β_{5d} have been measured by Kobrin *et al.* [17], McQuaide *et al.* [22], and Schönhense [13]. RRPA calculations [6] in the vicinity of the 5*d* threshold are larger than experiment for both the total photoionization cross section and the $\sigma(5d_{5/2})$ and $\sigma(5d_{3/2})$ partial cross sections.

The 4*f* cross section of Hg has also been the subject of experimental and theoretical studies. The partial cross section for photoionization from the 4*f* subshell has been measured by Lindle *et al.* [20] and found to be somewhat at variance with published RRPA [6] and Dirac-Slater calculations [23]. Branching ratios and asymmetry parameters have been measured by Kobrin *et al.* [17].

In light of the considerable interest taken in group-II*B* elements by experimentalists and theorists alike, it seems appropriate to present the results of a study of relaxation effects on inner-shell photoionization of all three elements Zn, Cd, and Hg. Such an approach (as was taken for group-II*A* elements [1]) helps to identify the systems for which relaxation effects can be expected to be significant. This survey also highlights strengths and limitations of the theory and suggests that, in at least one instance (Zn), the total absorption measurements [3] should be reexamined.

In Sec. II of this paper, the method used for the calculations is outlined. In Sec. III, we present the results of the present study and compare the theory with experiment. Section IV is a brief discussion of some of the implications of the work.

II. METHODS

The nonrelativistic random-phase approximation [usually called the random-phase approximation with exchange (RPAE)] [24] and the relativistic random-phase approximation [25] have been very successful at describing photoionization in many closed-shell atoms, especially the noble gases [26]. These techniques treat final-state intra- and interchannel interactions as well as some of the effects of virtually excited pairs of electrons in the ground and ionic configurations [27]. The photoionization spectra of valence shells of group-II*A* and group-II*B* elements, however, are dominated by double-electron resonances and theoretical methods which explicitly treat the complex interactions between the two valence electrons must be used for an accurate description. These methods include the multiconfiguration relativistic random-phase-approximation theory [28], the close-coupling technique [29,30], configuration interaction (CI) [31], the multiconfiguration Tamm-Dankoff approximation [32], the hyperspherical-coordinate approach [33], MBPT [34], and the eigenchannel *R*-matrix theory combined with the multichannel quantum-defect theory [35]. Although these CI effects limit the effectiveness of RPAE and RRPA calculations for the valence subshell cross sections of group-II*A* and group-II*B* atoms, the many-electron $(n-1)d^{10}$ inner-subshell cross sections are affected by

the multiconfiguration initial state of the few-electron outer ns^2 subshell in second and higher order of perturbation theory only. Photoionization-with-excitation channels are also not explicitly accounted for within the RPAE and RRPA methods. Thus one may expect the gross features of inner-shell photoionization to be well described by either RPAE or RRPA; however, neither double-electron resonances, which may occur within a few eV above the inner-shell threshold, nor the displacement of oscillator strength from single-excitation channels to multiply excited channels is accounted for. These important limitations of the theory must be considered when comparing the results presented here.

A detailed description of the RRPA has been given by Johnson and Lin [25]. Here we point out that, in the RRPA, the partial photoionization cross section at photon energy ω for a given subshell $n\kappa$ is (in atomic units) given by

$$\sigma_{n\kappa}(\omega) = \frac{4\pi^2 \alpha\omega}{3} (|D_{nj \to j-1}|^2 + |D_{nj,j}|^2 + |D_{nj,j+1}|^2) ,$$

(1)

where n is the principal quantum number and $\kappa = \mp(j+1/2)$ for $j = l \pm \frac{1}{2}$, with j and l being the single-electron total and orbital angular momentum quantum numbers, respectively. The dipole amplitude for channel $nj \to j'$ is represented by $D_{nj \to j'}$. The angular-distribution asymmetry parameter, $\beta_{n\kappa}$ for subshell $n\kappa$, is defined in terms of the differential cross section

$$\frac{d\sigma_{n\kappa}(\omega)}{d\Omega} = \frac{\sigma_{n\kappa}(\omega)}{4\pi} \left[1 - \frac{\beta_{n\kappa}(\omega)}{2} P_2(\cos\theta) \right] ,$$

(2)

with $d\Omega$ being the infinitesimal element of solid angle of the photoelectron and the angle θ defined as the angle between the directions of photon flux and photoelectron momentum vector. The form for β which will be presented in Sec. III will be the average of the $\beta_{n\kappa}$'s for a given nl shell, weighted by the photoionization cross section, i.e.,

$$\beta_{nl} = \frac{\displaystyle\sum_{\substack{\kappa = -(l+1), l \\ \kappa \neq 0}} \beta_{n\kappa}\sigma_{n\kappa}}{\displaystyle\sum_{\substack{\kappa = -(l+1), l \\ \kappa \neq 0}} \sigma_{n\kappa}} .$$

(3)

The calculations presented here were performed using the truncated RRPA. This leads to a loss of gauge invariance; however, enough channels were included in the RRPA calculations to ensure agreement between the "length" and "velocity" forms of the cross section to within a few percent. The cross-section results presented in the figures will be geometric means of length and velocity. The following fifteen channels were included in the calculations in the vicinity of the $(n-1)d$ thresholds of Zn $(n=4)$, Cd $(n=5)$, and Hg $(n=6)$:

$ns_{1/2} \rightarrow \epsilon p_{1/2}, \epsilon p_{3/2}$,

$(n-1)d_{5/2} \rightarrow \epsilon p_{3/2}, \epsilon f_{3/2}, \epsilon f_{5/2}$,

$(n-1)d_{3/2} \rightarrow \epsilon p_{1/2}, \epsilon p_{3/2}, \epsilon f_{5/2}$,

$(n-1)p_{3/2} \rightarrow \epsilon s_{1/2}, \epsilon d_{3/2}, \epsilon d_{5/2}$,

$(n-1)p_{1/2} \rightarrow \epsilon s_{1/2}, \epsilon d_{3/2}$,

$(n-1)s_{1/2} \rightarrow \epsilon p_{1/2}, \epsilon p_{3/2}$.

Above the threshold for $4f$ photoionization of Hg, we used the 19 dipole-allowed channels

$6s_{1/2} \rightarrow \epsilon p_{1/2}, \epsilon p_{3/2}$,

$5d_{5/2} \rightarrow \epsilon p_{3/2}, \epsilon f_{3/2}, \epsilon f_{5/2}$,

$5d_{3/2} \rightarrow \epsilon p_{1/2}, \epsilon p_{3/2}, \epsilon f_{5/2}$,

$5p_{3/2} \rightarrow \epsilon s_{1/2}, \epsilon d_{3/2}, \epsilon d_{5/2}$,

$5p_{1/2} \rightarrow \epsilon s_{1/2}, \epsilon d_{3/2}$,

$4f_{7/2} \rightarrow \epsilon d_{5/2}, \epsilon g_{7/2}, \epsilon g_{9/2}$,

$4f_{5/2} \rightarrow \epsilon d_{3/2}, \epsilon d_{5/2}, \epsilon g_{7/2}$.

The importance of core relaxation in inner-shell photoionization has been noted by many workers in a number of systems. Amusia included this effect in the RPAE method in an approximate way by assuming that the relaxation is complete and calculating continuum orbitals in the potential of the relaxed ionic orbitals rather than in the potential of frozen-core neutral atom orbitals [the

method has been referred to as the generalized RPAE (GRPAE)] [24]. The RRPA code of Johnson and Lin [25] was similarly modified to include these relaxation effects (the RRPAR) [2]. Since, in the model, the relaxed-core orbitals are used, it is as though the relaxation occurs instantaneously. The photoelectron-energy dependence of the extent of relaxation is neglected and the relaxed potential is expected to be less realistic than the frozen-core potential at higher photoelectron energies.

There is some arbitrariness as to which of the j levels of a subshell should contain the hole for the relaxed ion calculation. We have assumed that the hole is in the level with $j=l+\frac{1}{2}$ since this level has a lower threshold energy and a larger occupation number than the level with $j=l-\frac{1}{2}$.

In calculating partial cross sections with relaxed orbitals, we include overlap integrals $\Pi \langle \phi_i' | \phi_i \rangle^{q_i}$ between the ground-state orbitals ϕ_i and the corresponding orbitals of the final state ϕ_i' in the RRPAR matrix element for each subshell i of the ion with occupation number q_i [2]. According to the "sudden approximation" [36], the overlap integrals account, in an approximate energy-independent manner, for the transfer of photoabsorption oscillator strength from the single-excitation channel to multiply excited channels such as photoionization with excitation and double photoionization.

The thresholds normally used in RRPA calculations are the Dirac-Hartree-Fock (DHF) eigenvalues [25]. Kelly has pointed out [37] that including the all-orders

TABLE I. Photoionization thresholds in a.u. for subshells of group-IIB atoms included in the present calculations. Column four lists absolute values of single-particle eigenvalues from Dirac-Hartree-Fock (DHF) calculations used for thresholds in the RRPA calculations. Column five lists the differences of self-consistent DHF calculations for the ground state and the ionic state. The experimental values are from Ref. [38].

Atom	Subshell	J	Threshold		
			DHF	ΔE_{SCF}	Expt.
Zn	$3s$	1/2	5.800		
	$3p$	1/2	3.958		3.63
	$3p$	3/2	3.837		3.53
	$3d$	3/2	0.771	0.547	0.6431
	$3d$	5/2	0.755	0.535	0.6310
	$4s$	1/2	0.299		0.345
Cd	$4s$	1/2	4.747		
	$4p$	1/2	3.271		
	$4p$	3/2	3.046		
	$4d$	3/2	0.738	0.618	0.6718
	$4d$	5/2	0.709	0.592	0.6460
	$5s$	1/2	0.281		0.330
Hg	$5s$	1/2	5.103		4.924
	$4f$	5/2	4.473	3.994	4.079
	$4f$	7/2	4.312	3.841	3.939
	$5p$	1/2	3.537		3.32
	$5p$	3/2	2.842		2.63
	$5d$	3/2	0.650	0.556	0.6137
	$5d$	5/2	0.575	0.489	0.5454
	$6s$	1/2	0.328		0.3833

sum of certain classes of MBPT diagrams leads to a shift in the threshold from the Hartree-Fock eigenvalue to the fully correlated result. In the GRPAE or RRPAR, the difference between the total self-consistent energy of the ground state and the total self-consistent energy of the ion ($\Delta E_{\rm SCF}$) or the experimental threshold energy is normally used for the channel for which core relaxation is being considered [2]. In the strict RRPA calculations we have utilized DHF threshold energies, while in the RRPAR calculations we have used experimental thresholds. The DHF and experimental (where available from photoelectron spectroscopy [38]) threshold energies relevant to the present calculations of group-II*B* elements are listed in Table I. The $\Delta E_{\rm SCF}$ energies are also listed for comparison purposes for the channels in which core relaxation was included.

III. RESULTS

A. Zinc

In Fig. 1(a) we present the total photoionization cross sections for atomic zinc above the $3d_{5/2}$ threshold. The RRPA result is the sum of the single-excitation channels $4s_{1/2}+3d_{3/2}+3d_{5/2}+3p_{1/2}+3p_{3/2}+3s_{1/2}$. The RRPA result shown here is similar to that previously reported by Johnson, Radojević, and Deshmukh [6] except that the $3p_{1/2,3/2}$ and $3s_{1/2}$ channels were not included in the former calculation. Calculations were not performed for energies within a few eV below thresholds since it is known that autoionizing resonances will be present in those regions and the RRPA code will not readily converge. The results including core relaxation (RRPAR)
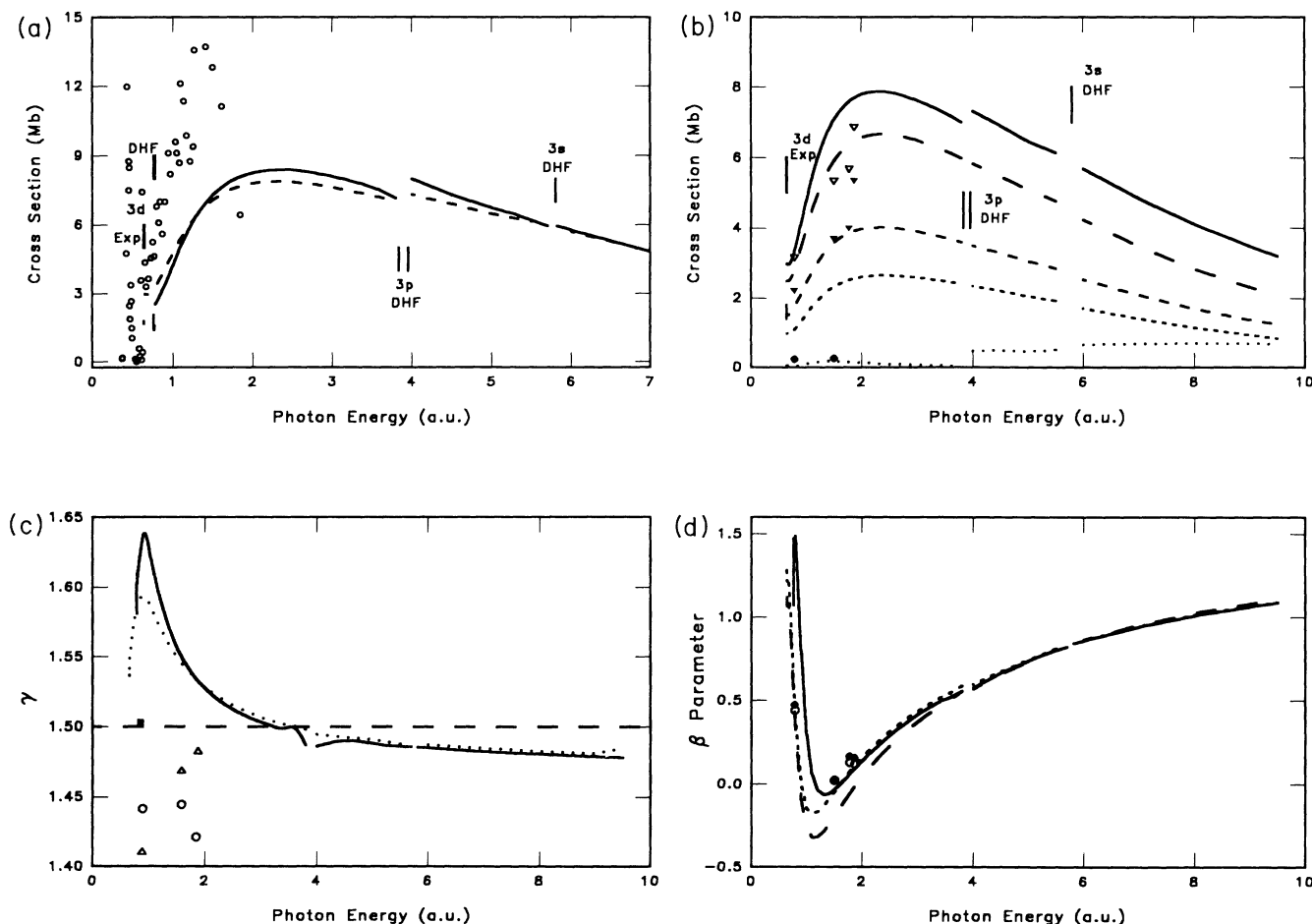

FIG. 1. Photoionization parameters above the $3d$ thresholds for atomic zinc. (a) Total photoionization cross sections in the RRPA (solid line) and RRPAR (dashed line). Experimental data points (open circles) are from Harrison, Schoen, and Cairns [3]. (b) Total photoionization cross section (solid line), sum of $3d_{5/2}$ and $3d_{3/2}$ partial cross sections (long-dashed line), $3d_{5/2}$ partial cross section (medium-dashed line), $3d_{3/2}$ partial cross section (short-dashed line), and sum of other single-excitation channels (dotted line) in the RRPAR. Open triangles, closed triangles, and closed circles represent experimentally measured $3d_{5/2}$, $3d_{3/2}$, and $3s$ partial cross sections [4], respectively. (c) Branching ratios $\gamma=\sigma(3d_{5/2})/\sigma(3d_{3/2})$ in the RRPA (solid line) and the RRPAR (dotted line). Experiment represented by open circles [4], solid square [5], and open triangles [11]. (d) Photoelectron angular-distribution asymmetry parameters β_{3d} in the RRPA length form (solid line) and in the RRPAR length (long-dashed line) and the RRPAR velocity (short-dashed line) forms. Closed and open circles represent, respectively, experimental $3d_{5/2}$ and $3d_{3/2}\beta$ parameters from Ref. [4].

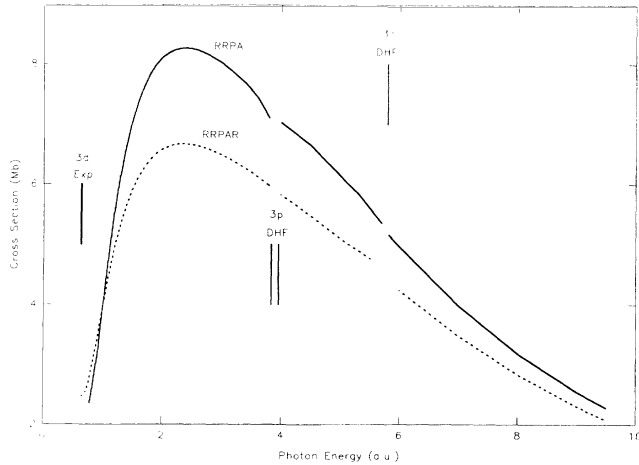KUTZNER, TIDWELL, VANCE, AND RADOJEVIĆ

FIG. 2. Partial $3d$ photoionization cross sections in the RRPA (solid line) and RRPAR (dashed line).

are the sum of the single-excitation channels listed above with the determinant of overlap integrals not included in the matrix elements; thus oscillator strength from both singly and doubly excited channels are included in the total photoionization cross section.

For comparison, we have plotted the experimental measurements of Harrison, Schoen, and Cairns [3], who measured the relative cross sections in this region using a mass spectrometer and a sodium salicylate-coated detector. The measured cross section was put on an absolute scale by normalization to data measured from the valence threshold to 16.5 eV by Marr and Austin [39]. They are reported to be accurate to approximately 10% [40]. Neither the scale of the theoretical cross sections nor the shape appears to agree with the experimental results which peak somewhat earlier than the theoretical cross sections. It has been shown [20], since the time of the zinc measurements, that the quantum yield of sodium sal-
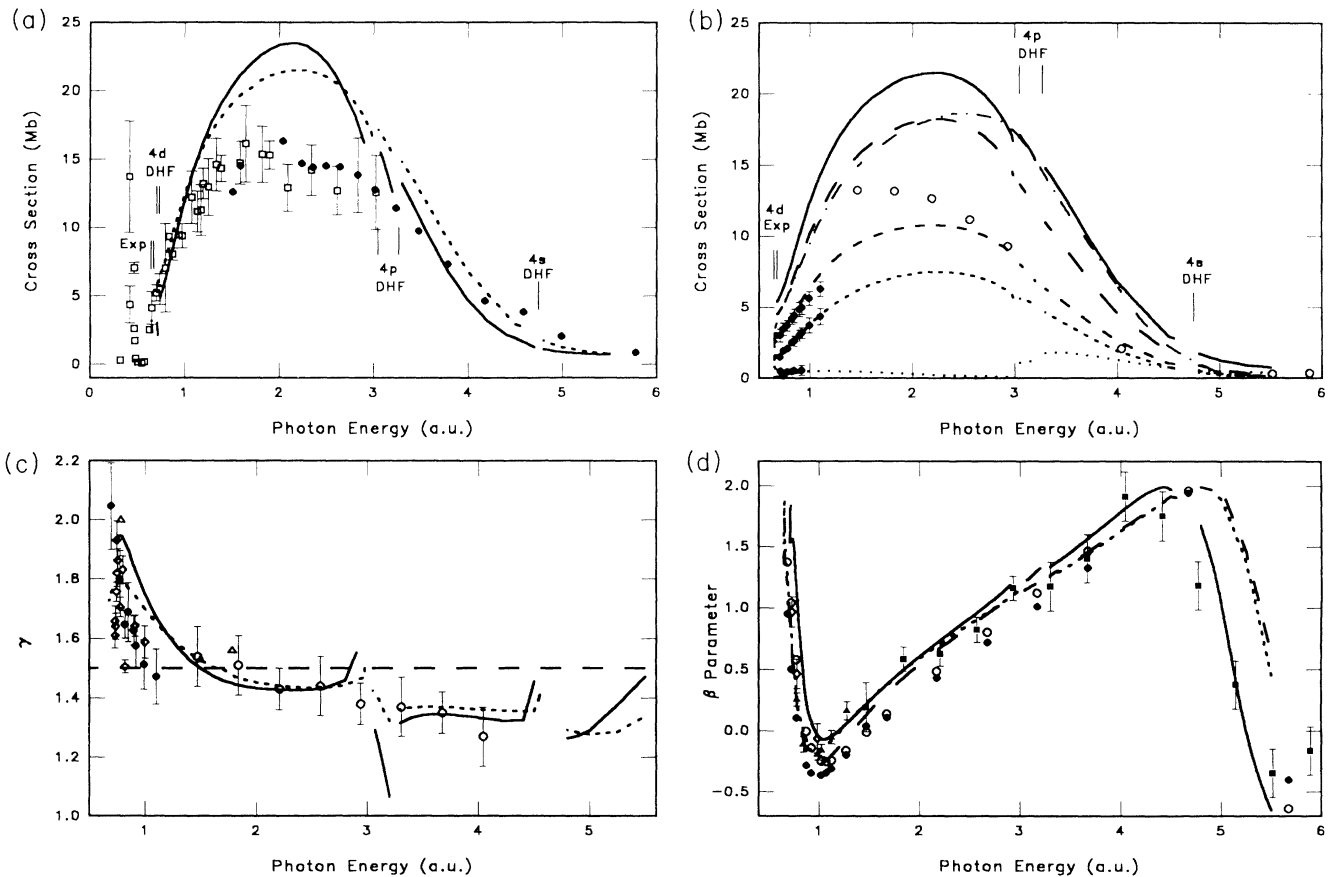

FIG. 3. Photoionization parameters above the $4d$ subshell thresholds of atomic cadmium. (a) Total photoionization cross sections in the RRPA (solid line) and RRPAR (dashed line). Experimental measurements are represented by closed circles [7] and open squares [8]. (b) Total photoionization cross section in the RRPAR (solid line). Partial $4d$ cross sections in the RRPAR (long-dashed line) and MBPT [15] (dot-dashed line); experimental partial $4d$ cross section [9] represented by open circles. Partial $4d_{5/2}$ and partial $4d_{3/2}$ cross sections in the RRPAR are represented by the medium-dashed line and the short-dashed line, respectively. Dotted curve represents the sum of other singly excited channels. Partial cross sections measured by Shannon and Codling [10] are shown as solid dots with error bars. (c) Branching ratios $\gamma = \sigma(4d_{5/2})/\sigma(4d_{3/2})$ in the RRPA (solid line) and the RRPAR (dashed line). Experimental data are represented by the solid square [5], open circles [9], closed circles [10], open triangles [11], and open diamonds [12]. (d) Photoelectron angular-distribution asymmetry parameters β_{4d} in the RRPA length (solid line), RRPAR length (long-dashed line), and RRPAR velocity (short-dashed line) forms. Experimental measurements are represented by solid squares [9], open diamonds [12], and closed triangles [13]. Open circles and closed circles represent measured $4d_{3/2}$ and $4d_{5/2}$ β parameters, respectively, as measured by Theodosiou et al. [14].
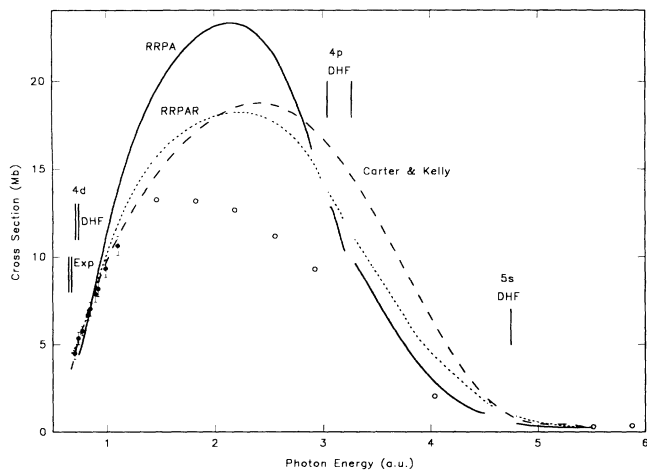
FIG. 4. Partial photoionization cross sections from the $4d$ subshell of cadmium. The solid curve represents the RRPA result; the short-dashed line represents the RRPAR result, the long-dashed line represents the MBPT calculations of Carter and Kelly [15]. The experimental data are represented by open circles [9] and closed circles [10].

icylate scintillators used as a photon-flux monitor increases at higher photon energies and it may be that corrections need to be applied to the measurements. The RRPA and RRPAR total photoionization cross sections differ slightly near the $3d$ thresholds and then converge to a common result at photon energies above approximately 6 a.u. This illustrates that a highly energetic photoelectron orbital is not strongly influenced by details of the ionic potential in which it is calculated.

In Fig. 1(b) the total RRPAR photoionization cross section is plotted along with the various partial cross sections. It is clear that the dominant contribution to the total photoionization cross sections comes from the $3d$ main-line channels. The sum of the various other single-excitation channels is seen to have an increasing share of the differential oscillator strength at higher energies. The reduction of the partial $3d$ cross section due to overlap integrals is 14%. This is a rough estimate of the absorption due to multiply excited channels. The experimentally determined partial cross sections of Süzer *et al.* [4] are also shown in Fig. 1(b). It should be noted that the experimental partial cross sections have been normalized to
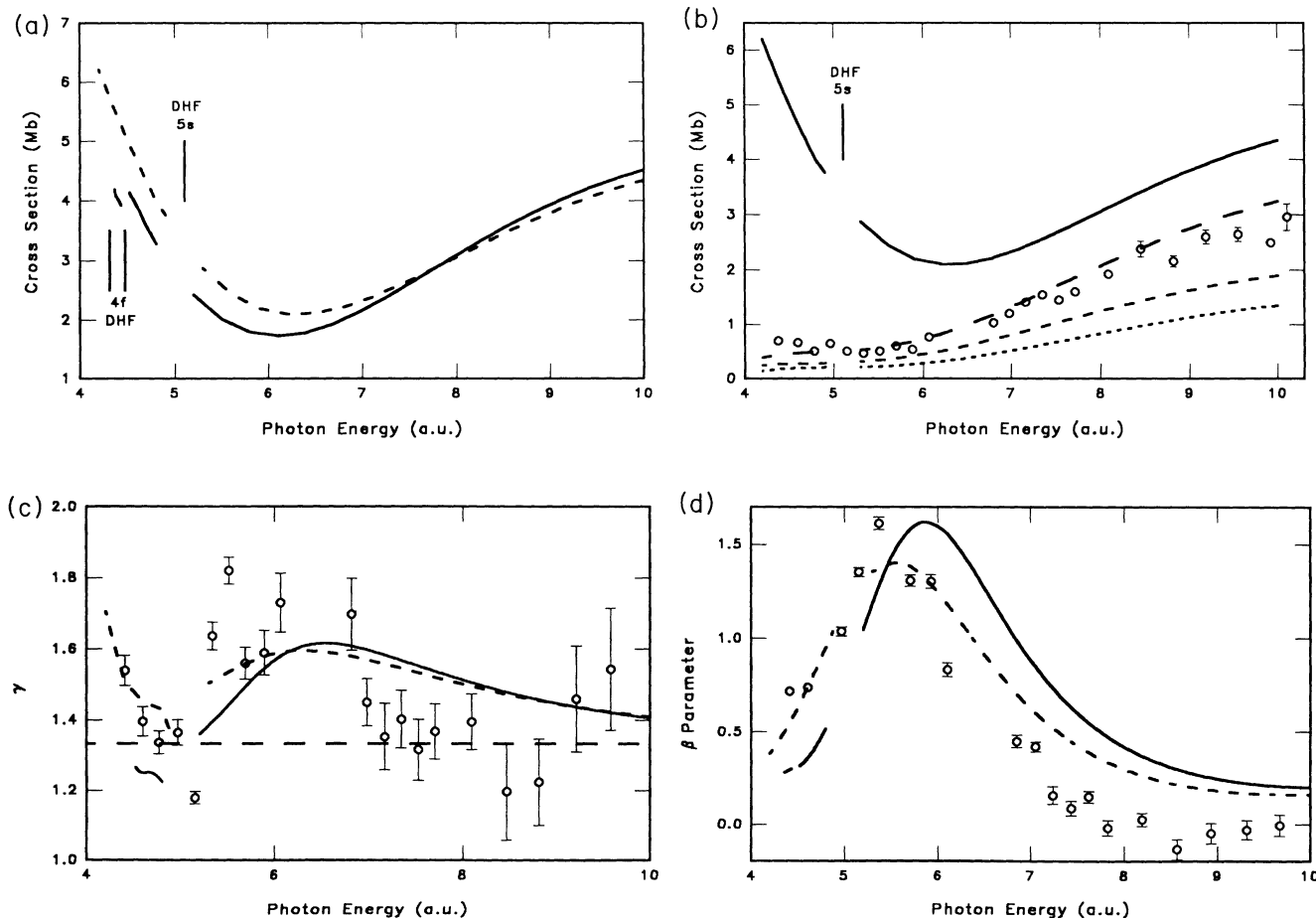

FIG. 5. Photoionization parameters above the $4f$ subshell thresholds for atomic mercury. (a) Total photoionization cross sections in the RRPA (solid line) and RRPAR (dashed line). (b) Total photoionization cross section (solid line), partial $4f$ cross section (long-dashed line), partial $4f_{7/2}$ cross section (medium-dashed line), and partial $4f_{5/2}$ cross section (short-dashed line) in the RRPAR. Experimentally measured points represented by open circles are from Lindle *et al.* [20]. (c) Branching ratios $\gamma = \sigma(4f_{7/2})/\sigma(4f_{5/2})$ in the RRPA (solid line) and the RRPAR (dashed line). Open circles represent the experimental data of Kobrin *et al.* [17]. (d) Photoelectron angular-distribution asymmetry parameters β_{4f} in the RRPA length (solid line), RRPAR (dashed line). Open circles are measurements [17].
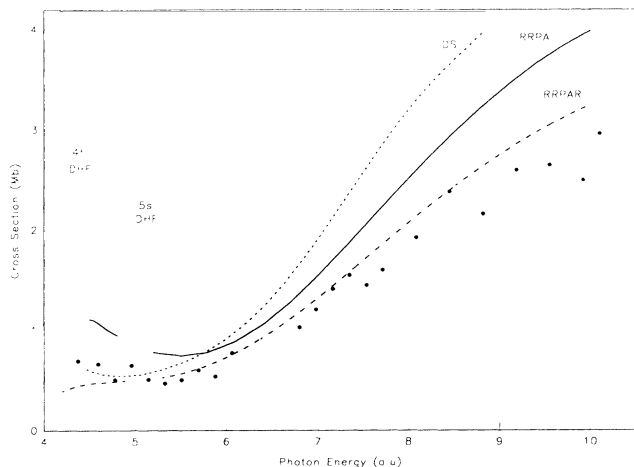
FIG. 6. Partial $4f$ photoionization cross sections for atomic mercury. The solid line is RRPA, the long-dashed line is RRPAR, and the short-dashed line is a Dirac-Slater calculation [23]. Closed circles represent the experimental results of Lindle *et al.* [20].

the total cross section measurement of Harrison, Schoen, and Cairns [3] [shown in Fig. 1(a)] at 0.779 a.u.

The branching ratios $\gamma = \sigma(3d_{5/2})/\sigma(3d_{3/2})$ are shown in Fig. 1(c) for both the RRPA and the RRPAR. Neither calculation agrees particularly well with the experiments [4,5,11]. The effect of relaxation on the angular-distribution asymmetry parameter β_{3d} is seen in Fig. 1(d). Both length and velocity forms of the asymmetry parameter are shown for the RRPAR because there is a significant difference in this case. The experimental β parameters [4] are consistent with both the RRPA and the RRPAR calculations.

Although the total photoionization cross section for zinc above the $3d$ threshold does not appear greatly altered by core relaxation, plots of the $3d$ partial cross sections in this energy region highlight more substantial differences; they are shown in Fig. 2. The RRPAR partial $3d$ cross section peaks at approximately 6.67 Mb rather than 8.26 Mb for the RRPA. Seventy-three percent of this difference is due to the reduction introduced by including overlap integrals; the residual difference is due to changes in the one-electron potential.

B. Cadmium

The total photoionization cross sections in the vicinity of the giant shape resonance above the $4d$ thresholds in atomic cadmium are shown in Fig. 3(a). The experimental data are from Cairns, Harrison, and Schoen [7] and Codling, Hamley, and West [8]. As has been noted in $4d$ photoionization of xenon, barium, and other elements, the effect of relaxation is to redistribute the oscillator

strength from the threshold region to higher photoelectron energies. Once again, the RRPA and the RRPAR results for the total cross sections converge at higher energies. It appears that both calculations are too large relative to the experiments at the cross section peak, a discrepancy which is not currently understood.

The total and partial cross sections in the RRPAR are plotted as a function of photon energy in Fig. 3(b) along with the MBPT result of Carter and Kelly [15] and the experiments of Shannon and Codling [10] and von Garnier *et al.* [9] The RRPAR results for the $4d_{5/2}$ and $4d_{3/2}$ partial cross sections are in excellent agreement with the measurements of Shannon and Codling [10]. Near the peak in the $4d$ partial cross section the theory is larger than the recent experimental measurements of von Garnier *et al.* [9]; however, the experimental result is a partitioning, using photoelectron spectroscopy, of the experimental total photoionization cross sections [7,8] shown in Fig. 3(a). Hence the lack of agreement between theory and experiment in the total cross sections gives a corresponding disagreement in the partial cross sections.

The branching ratios $\gamma = \sigma(4d_{5/2})/\sigma(4d_{3/2})$ for the RRPA and RRPAR are presented in Fig. 3(c). The numerous experimental results [5,9–12] are also plotted for comparison. Near the $4d$ thresholds, there are considerable differences between the results including relaxation effects (RRPAR) and the results which do not (RRPA), although it would be difficult to claim that one theory gives superior agreement with experiment. The branching ratio is lower near threshold for the RRPAR. The main reason for deviations of the branching ratio from the statistical value of $\gamma_{stat} = 3/2$ is a spin-orbit splitting of the $4d_{5/2}$ and $4d_{3/2}$ levels. Since both partial cross sections are monotonically increasing with increasing photon energy just above the $4d_{3/2}$ threshold, the $4d_{5/2}$ partial cross section which has a lower threshold has a larger value, above the $4d_{3/2}$ threshold, relative to the $4d_{3/2}$ partial cross section than that predicted by the statistical ratio. This trend continues until the peak of the $4d_{5/2}$ partial cross section after which point the $4d_{5/2}$ cross section is reduced slightly earlier than the $4d_{3/2}$ cross section. The effect of relaxation is to decrease the slope of each partial cross section near threshold, thus reducing the deviations of the branching ratio from the statistical value.

The angular-distribution asymmetry parameters β_{4d} are presented in Fig. 3(d). Both length and velocity results are shown for the RRPAR since the differences are significant near 1 a.u. It should be noted when the comparison is made with experiment [9,12–14] that for the RRPAR results experimental threshold energies were used and for the RRPA results the higher DHF eigenvalues were used.

To highlight the relaxation effects on the partial $4d$ cross section, in Fig. 4 we plot the partial cross sections in the RRPA, the RRPAR, and the MBPT [15] along with experiments [9,10]. Here the broadening and lowering of the peak of the shape resonance due to relaxation effects are clearly seen. The reduction in the $4d$ partial cross section of cadmium due to overlap integrals is approximately 10.7%.

C. Mercury $4f$

The total photoionization cross sections above the $4f$ thresholds of mercury for both the RRPA and the RRPAR are shown in Fig. 5(a). In the RRPAR, relaxation was assumed for the $4f$ hole and not for the $5d$ channels, which are still large in this region of the spectrum and couple strongly with the $4f$ cross section. The RRPAR cross section is larger than the RRPA near the $4f$ threshold, but by 10 a.u. is slightly less.

The total and partial $4f$ cross sections for the RRPAR are shown in Fig. 5(b) along with $4f$ partial cross section data by Lindle et al. [20]. The experimental data shown here include the important correction on previous measurements [17] for the increased quantum yield of the

sodium salicylate detector at higher energies.

The branching ratios $\gamma = \sigma(4f_{7/2})/\sigma(4f_{5/2})$ for the RRPA, the RRPAR, and experiment [17] are shown in Fig. 5(c). For energies just above the $4f_{5/2}$ threshold, the RRPAR predicts that the branching ratio should be greater than the statistical ratio $\gamma_{stat} = 4/3$, in agreement with experiment [17].

In Fig. 5(d), we present the RRPAR and RRPA results for the angular distribution parameter β_{4f} with the experimental results of Kobrin et al. [17]. In comparing the results it should again be noted that the thresholds used in the RRPAR calculation are approximately 0.38 a.u. lower than those used in the RRPA calculation.

The interesting interplay of many-body effects in the $4f$ cross section of mercury is apparent in Fig. 6. The Dirac-Slater calculation [23] shown there includes rela-
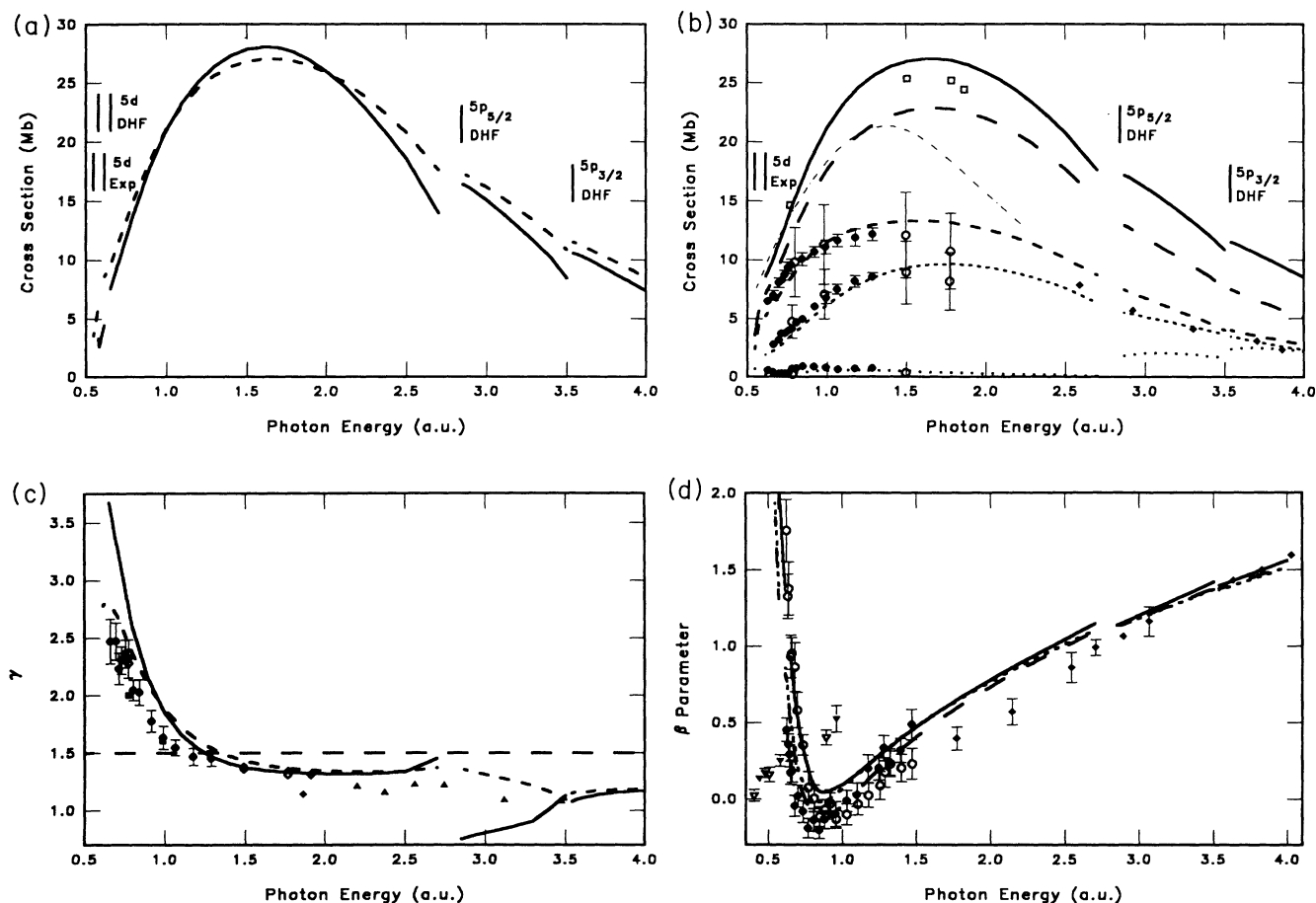

FIG. 7. Photoionization parameters above the $5d$ subshell thresholds of atomic mercury. (a) Total photoionization cross sections in the RRPA (solid line) and the RRPAR (dashed line). (b) Theory: total cross section (solid line), $5d$ partial cross section (long-dashed line), $5d_{5/2}$ partial cross section (medium-dashed line), $5d_{3/2}$ partial cross section (short-dashed line) and the sum of other single-excitation channels (dotted line) in the RRPAR. Experiment: open squares and dot-dashed line represent $5d$ partial cross sections of Refs. [4] and [18], respectively. Closed circles represent partial cross section measurements of Shannon and Codling [10] and open circles represent partial cross sections of Dehmer and Berkowitz [19]. Closed diamonds represent the $5d$ partial cross section reported by Lindle et al. [20]. (c) Branching ratios $\gamma = \sigma(5d_{5/2})/\sigma(5d_{3/2})$ in the RRPA (solid line) and the RRPAR (dashed line). Experimental measurements are represented by solid diamonds [4], solid circles [10], open diamonds [11], solid triangles [17], solid squares [19], and open squares [21]. (d) Photoelectron angular-distribution asymmetry parameter β_{5d} in the RRPA length (solid curve), RRPAR length (long-dashed curve), and RRPAR velocity (short-dashed curve) forms. Experiment: Open and closed triangles are $5d_{3/2}$ and $5d_{5/2}$ β parameters, respectively, measured by Schönhense [13]. Open and closed circles are $5d_{3/2}$ and $5d_{5/2}$ β parameters, respectively, measured by McQuaide et al. [22]. Closed diamonds represent the measurements of Kobrin et al. [17].
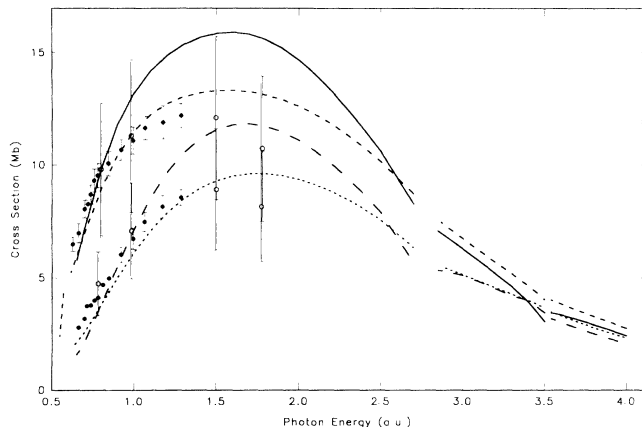
FIG. 8. Partial cross sections for photoionization from the $5d$ subshell of atomic mercury. Theory: solid line (long-dashed line) is the $5d_{5/2}$ ($5d_{3/2}$) partial cross section in the RRPA whereas the medium-dashed line (short-dashed line) is the $5d_{5/2}$ ($5d_{3/2}$) partial cross section in the RRPAR. Experiment: solid circles represent the partial $5d_{5/2}$ and $5d_{3/2}$ partial cross section measurements of Shannon and Codling [10] and open circles are from Dehmer and Berkowitz [19].

tivistic effects but does not include interchannel coupling between the $4f$ channels and the important $5d$ channel; also, the exchange potential is treated approximately in the Dirac-Slater model. The RRPA calculation includes interchannel coupling which accounts for the increase in the $4f$ partial cross section near the threshold. The effects of core relaxation can be seen in the RRPAR result, which is considerably reduced near threshold relative to the RRPA calculation. At higher energies the RRPAR cross section is in better agreement with experiment due partly to the (approximately 14%) reduction from the inclusion of overlap integrals which roughly accounts for the transfer of oscillator strength from the main-line channels to photoionization-with-excitation channels.

D. Mercury $5d$

Total photoionization cross sections above the $5d$ threshold for atomic mercury are shown in Fig. 7(a) for both the RRPA and the RRPAR. The effects of interchannel coupling are seen near the thresholds for $5p$ photoionization. Although the total cross sections do not appear very different in this plot, some of the other photoionization parameters are more strongly affected.

In Fig. 7(b) the total RRPAR cross section is shown along with the partial cross sections for $5d_{5/2}$ and $5d_{3/2}$ and the remaining single-photoionization channels. The

experimental measurements of many workers [4,10,18–20] are also shown for comparison. The agreement between theory and experiment is very good near threshold; however, at higher energies the theory is larger than experiment.

The branching ratios $\gamma = \sigma(5d_{5/2})/\sigma(5d_{3/2})$ for mercury calculated in the RRPA and RRPAR are plotted in Fig. 7(c). Also plotted are the results of several experimental measurements [4,10,11,17,19,21]. The RRPAR branching ratio is lower in value near the $5d_{3/2}$ threshold than the RRPA and in better agreement with experiments; this is again because of the delay of the onset of photoabsorption above threshold due to relaxation effects. Angular-distribution asymmetry parameters β_{5d} for the length form in the RRPA and in length and velocity forms in the RRPAR are shown along with experiment [13,17,22] in Fig. 7(d). Both calculations are in reasonable agreement with the experimental measurements of McQuaide et al. [22], but would appear to disagree with those of Schönhense [13].

In Fig. 8, the RRPA and RRPAR partial cross sections $\sigma(5d_{5/2})$ and $\sigma(5d_{3/2})$ are plotted together along with the experimental partial cross sections of Shannon and Codling [10] and Dehmer and Berkowitz [19]. Some of the differences between the two calculations can be attributed to the reduction due to overlap integrals which is an energy-independent reduction of 7.5%. Differences in the slope of the cross sections may also be noted in the partial cross sections.

IV. CONCLUSION

The RRPAR method has been compared and contrasted with the RRPA and with the experiments for inner-shell photoionization of group-IIB elements. The inclusion of relaxation has improved agreement with experiment most notably for mercury $4f$ and $5d$ photoionization. For atomic cadmium, we have confirmed the reported results of MBPT [15] showing the need to include relaxation in calculations of the $4d$ cross section. The measured cadmium cross sections are generally somewhat lower at the peak than are the calculations. The largest discrepancy between theory and experiment is in the $3d$ cross section of zinc; this problem warrants further experimental and theoretical investigation.

ACKNOWLEDGMENTS

[1] M. Kutzner, D. Winn, and S. Mattingly, Phys. Rev. A **48**, 404 (1993).

[2] V. Radojević, M. Kutzner, and H. P. Kelly, Phys. Rev. A **40**, 727 (1989).

[3] H. Harrison, R. I. Schoen, and R. B. Cairns, J. Chem. Phys. **50**, 3930 (1969).

[4] S. Süzer, P. R. Hilton, N. S. Hush, and S. Nordholm, J. Electron Spectrosc. Relat. Phenom. **12**, 357 (1977).

[5] T. E. H. Walker, J. Berkowitz, J. L. Dehmer, and J. I. Waber, Phys. Rev. Lett. **31**, 678 (1973).

[6] W. R. Johnson, V. Radojević, P. Deshmukh, and K. T. Cheng, Phys. Rev. A **25**, 337 (1982).

[7] R. B. Cairns, H. Harrison, and R. I. Schoen, J. Chem. Phys. **51**, 5440 (1969).

[8] K. Codling, J. R. Hamley, and J. B. West, J. Phys. B **11**, 1713 (1978).

[9] V. von Garnier, G. Langer, J. Viefhaus, R. Wehlitz, and U. Becker (unpublished).

[10] S. P. Shannon and K. Codling, J. Phys. B **11**, 1193 (1978).

[11] S. Süzer, S.-T. Lee, and D. A. Shirley, Phys. Rev. A **13**, 1842 (1976).

[12] P. H. Kobrin, U. Becker, S. Southworth, C. M. Truesdale, D. W. Lindle, and D. A. Shirley, Phys. Rev. A **26**, 842 (1982).

[13] G. Schönhense, J. Phys. B **14**, L187 (1981).

[14] C. E. Theodosiou, A. F. Starace, B. R. Tambe, and S. T. Manson, Phys. Rev. A **24**, 301 (1981).

[15] S. L. Carter and H. P. Kelly, J. Phys. B **11**, 2467 (1978).

[16] B. R. Tambe, W. Ong, and S. T. Manson, Phys. Rev. A **23**, 799 (1981).

[17] P. H. Kobrin, P. A. Heimann, H. G. Kerkhoff, D. W. Lindle, C. M. Truesdale, T. A. Ferrett, U. Becker, and D. A. Shirley, Phys. Rev. A **27**, 3031 (1983).

[18] R. B. Cairns, H. Harrison, and R. I. Schoen, J. Chem. Phys. **53**, 96 (1970).

[19] J. L. Dehmer and J. Berkowitz, Phys. Rev. A **10**, 484 (1974).

[20] D. W. Lindle, T. A. Ferrett, P. A. Heimann, and D. A. Shirley, Phys. Rev. A **34**, 1131 (1986).

[21] D. C. Frost, C. A. McDowell, and D. A. Vroom, Chem. Phys. Lett. **1**, 93 (1967).

[22] B. H. McQuaide, M. S. Banna, P. Gerard, and M. O. Krause, Phys. Rev. A **35**, 1603 (1987).

[23] B. R. Tambe and S. T. Manson, Phys. Rev. A **30**, 256

[24] M. Ya. Amusia, *Atomic Photoeffect,* translated by K. T. Taylor (Plenum, New York, 1990).

[25] W. R. Johnson and C. D. Lin, Phys. Rev. A **20**, 964 (1979).

[26] W. R. Johnson and K. T. Cheng, Phys. Rev. A **20**, 978 (1979).

[27] A. F. Starace, in *Corpuscles and Radiation in Matter I,* edited by W. Mehlhorn, Handbuch der Physik Vol. 31 (Springer-Verlag, Berlin, 1982), p. 75.

[28] K.-N. Huang and W. R. Johnson, Phys. Rev. A **25**, 634 (1982); W. R. Johnson and K.-N. Huang, Phys. Rev. Lett. **48**, 315 (1982).

[29] D. L. Moores, Proc. Phys. Soc. London **91**, 830 (1967); **88**, 843 (1966).

[30] P. Scott, A. E. Kingston, and A. Hibbert, J. Phys. B **16**, 1983.

[31] P. L. Altick, Phys. Rev. **169**, 21 (1968).

[32] V. Radojević and W. R. Johnson, Phys. Rev. A **31**, 2991 (1985).

[33] C. H. Greene, Phys. Rev. A **23**, 661 (1981).

[34] H. P. Kelly, Phys. Rev. B **136**, 896 (1964); Z. Altun, S. L. Carter, and H. P. Kelly, Phys. Rev. A **27**, 1943 (1983); D. Frye and H. P. Kelly, J. Phys. B **20**, L677 (1987); Z. Altun, Phys. Rev. A **40**, 4968 (1989).

[35] C. H. Greene and M. Aymar, Phys. Rev. A **44**, 1773 (1991).

[36] T. Åberg, in *Photoionization and Other Probes of Many-Electron Interactions,* edited by F. Wuilleumier (Plenum, New York, 1976), pp. 49–59.

[37] H. P. Kelly, Adv. Theor. Phys. **2**, 75 (1968).

[38] H. Siegbahn and L. Karlsson, in *Corpuscles and Radiation in Matter I,* (Ref. [27]), p. 215.

[39] G. V. Marr and J. M. Austin, J. Phys. B **2**, 107 (1969).

[40] J. A. R. Samson, in *Corpuscles and Radiation in Matter I* (Ref. [27]), p. 177.

(1984).